PROCEEDINGS OF SPIE

SPIEDigitalLibrary.org/conference-proceedings-of-spie

Stray light suppression of a compact off-axis telescope for a satellite-borne instrument for atmospheric research

Arvid Hammar, Ole Martin Christensen, Woojin Park, Soojong Pak, Anders Emrich, et al.

Arvid Hammar, Ole Martin Christensen, Woojin Park, Soojong Pak, Anders Emrich, Jan Stake, "Stray light suppression of a compact off-axis telescope for a satellite-borne instrument for atmospheric research," Proc. SPIE 10815, Optical Design and Testing VIII, 108150F (5 November 2018); doi: 10.1117/12.2500555

SPIE.

Event: SPIE/COS Photonics Asia, 2018, Beijing, China

Stray Light Suppression of a Compact Off-Axis Telescope for a Satellite-Borne Instrument for Atmospheric Research

Arvid Hammar[a,b,*], Ole Martin Christensen[c], Woojin Park[d], Soojong Pak[d], Anders Emrich[a], and Jan Stake[b]

[a]Omnisys Instruments AB, August Barks gata 6B, SE-421 32 Västra Frölunda, Sweden
[b]Terahertz and Millimetre Wave Laboratory, Department of Microtechnology and Nanoscience – MC2, Chalmers University of Technology, SE-412 96 Gothenburg, Sweden
[c]Department of Meteorology, Stockholm University, 106 91, Stockholm, Sweden
[d]School of Space Research, Kyung Hee University, 1732 Deokyoungdaero, Giheung-gu, Yongin-si, Gyeonggi-do 17104, Republic of Korea

ABSTRACT

In this study, simulations and measurements were used to investigate stray light properties of the three-mirror off-axis telescope of a new satellite for atmospheric research called Mesospheric Airglow/Aerosol Tomography Spectroscopy (MATS). A 700 mm breadboard baffle for stray light rejection has been designed and tested. Good performance was achieved by coating the baffle's inside with Vantablack S-VIS®, which has a hemispherical reflectance of 0.2-0.6% across the instrument's detection band (270-776 nm). A point source transmittance (PST) down to 10^{-6} was measured for the full-size baffle breadboard. This is in excellent agreement with simulations performed in OpticStudio/LightTools, where scattering was modeled using empirical BRDF data. From the breadboard results, a simulation model of a flight-representative prototype model of the entire instrument was set up in OpticStudio. Strong signals just outside the field of view constitute the biggest challenge, where a PST in the order of $10^{-6} - 10^{-4}$ is required. Simulations suggest that the PST of the prototype limb instrument will be lower than this. Adding to these simulations, an instrument model was developed, which will be utilized by the end-users to remove unwanted features in the data stemming from the instrument itself. Besides stray light, the model also takes into account the most relevant aspects of the instrument, such as image resolution (from measured/simulated point spread functions), image sensor characteristics as well as temperature and wavelength dependencies.

Keywords: stray light, Vantablack, off-axis telescope, MATS, PST, instrument modeling, stray light measurements, satellite

1. INTRODUCTION

Mesospheric Airglow/Aerosol Tomography and Spectroscopy (MATS) is an upcoming Swedish satellite mission scheduled for launch Q4 2019.[1] Its goal is to study the layer of the atmosphere called mesosphere/lower thermosphere, located roughly between altitudes 70-110 km. In particular, it will investigate atmospheric buoyancy waves, also called gravity waves (not to be confused with *gravitational waves*), in noctilucent clouds and oxygen A-band airglow in order to improve the understanding of atmospheric dynamics and of how these waves affect the large scale wind patterns around the globe.[2] To observe these phenomena, the MATS satellite is designed to observe the sky from a limb viewing geometry, i.e. looking sideways through the atmosphere from space (see Figure 1). Using scattered sunlight at 270 and 300 nm, it will take images of noctilucent clouds from different angles and by using tomographic reconstruction techniques, three-dimensional structures in these clouds can be retrieved. Similarly, images of the oxygen A-band airglow at several wavelengths around 762 nm will be captured and, by using the spectral information, it is possible to retrieve information about the atmospheric temperature in the region of interest.

Further author information: (Send correspondence to Arvid Hammar)
Arvid Hammar: E-mail: arvid.hammar@omnisys.se, Telephone: +46 722 07 2739

Optical Design and Testing VIII, edited by Yongtian Wang, Tina E. Kidger, Kimio Tatsuno, Proc. of SPIE Vol. 10815, 108150F · © 2018 SPIE
CCC code: 0277-786X/18/$18 · doi: 10.1117/12.2500555

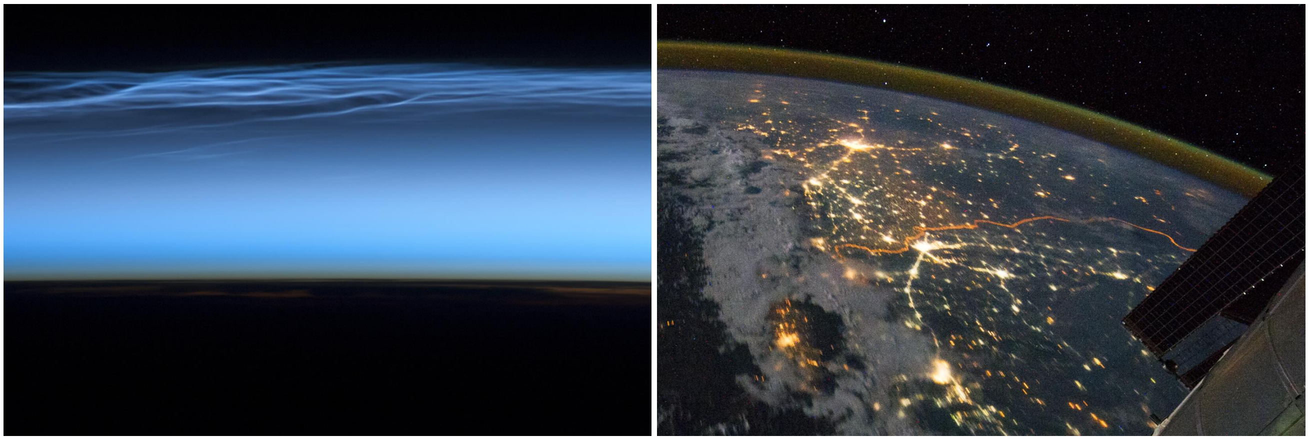

Figure 1. Image of wave structures in noctilucent clouds (left) and airglow (right) on the limb of the atmosphere. Pictures are taken from the International Space Station (ISS) (Credit: NASA).

As seen in Figure 1, airglow and noctilucent clouds can easily be measured at night when seen against the contrast of space. However, during daytime, the solar light reflected off the surface of the earth poses a significant challenge in terms of stray light for instruments of this kind.[3–5] In fact, upwelling radiation from the Earth's surface is several orders of magnitude larger than the desired signal. In addition, direct solar illumination of the satellite platform – although far from the instrument's optical axis – can also cause serious stray light problems. For this reason, a significant attenuation of stray light is needed to ensure that the captured images retain a high enough contrast for scientific analysis. Hence, it is very important to carefully characterize the instrument's stray light suppression capabilities – especially in the regions with the strongest sources of unwanted light.

This paper will describe how a flight-representative prototype limb instrument was designed to achieve sufficient stray light rejection, as well as results from initial tests and simulations to confirm that the design holds up to its specifications. Finally, the in-orbit performance of the instrument will be evaluated based on an end-to-end software simulator.

2. LIMB INSTRUMENT AND STRAY LIGHT REQUIREMENTS

The limb instrument is based on a single off-axis three-mirror reflective telescope (f/D = 7.3) with a field of view (FOV) of 5.67° × 0.91°. A network of beamsplitters and filters are used to form images in six separate detection channels, cf. Table 1. All channels use passively cooled back-lit CCD sensors (Teledyne E2V -CCD4210) with corresponding anti-reflective coatings.[6]

channel	UV1	UV2	IR1	IR2	IR3	IR4
center wavelength (nm)	270.0	304.5	762.0	763.0	754.0	772.0
bandwidth (nm)	3.0	3.0	3.5	8.0	3.0	3.0

Table 1. Center wavelengths and bandwidths of the six channels of the limb instrument. Bandwidths are defined as full width half maximum measured from peak transmission.

Figure 2 shows the optical system and its mechanical implementation, as well as how light propagates through the system through a network of beamsplitters and filters. A total of 16 flat glass components (5 beamsplitters, 3 broadband filters, 2 folding mirrors and 6 narrowband filters) are used to achieve the desired spectral selection while preserving good imaging performance. Directly following the tertiary mirror M3 is a beamsplitter that reflects wavelengths below 345 nm while longer wavelengths are transmitted. The spectral selection for each channel (c.f. Table 1) is then accomplished using broadband filters and individual narrowband filters in front of each image sensor.

In order to efficiently suppress stray light, a long baffle structure is placed in front of the primary mirror M1. This baffle is coated with Vantablack S-VIS®, which is an extremely black coating based on vertically

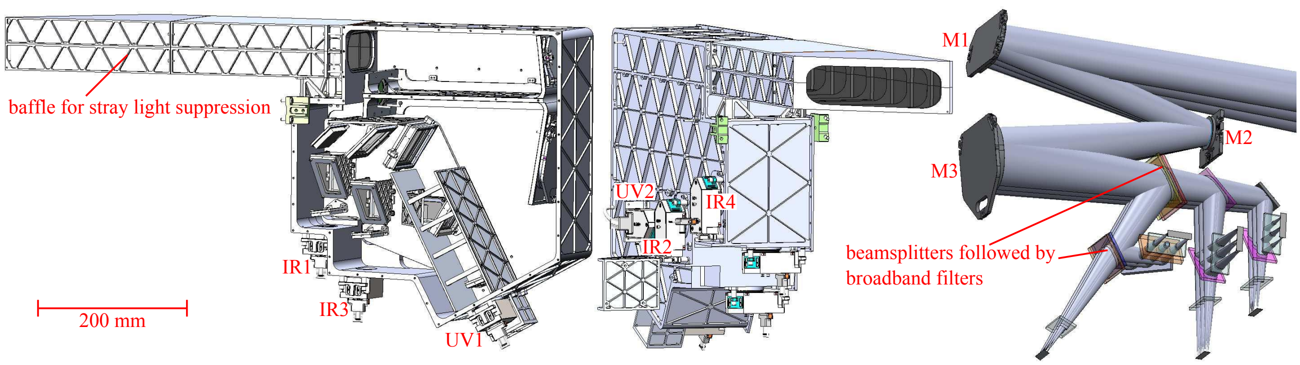

Figure 2. Mechanical implementation with one of the side covers removed to expose the instrument's inside (left and middle) and optical layout of the limb instrument (right). The location of the image sensors of the six channels (UV1-UV2 and IR1-IR4) are indicated in red. The three mirrors of the telescope are denoted M1-M3.

aligned carbon nanotubes. On average, this coating has a reflectance between 0.2-0.6% in the wavelength region 250-1400 nm.[7] The housing and all other structures supporting optical components use a black nickel coating, which has a reflectivity of 2-6%. Although preferable from a stray light perspective, the telescope does not feature a field stop, which can be used to block out stray light just outside the FOV. Instead, Lyot stops are used in front of each image sensor. In addition, with the sensors being deeply embedded in the structure, all critical paths from the primary M1 and secondary M2 mirrors are removed. However, it has been shown that telescopes of this kind with the aperture stop at the secondary mirror can become a considerable contributor to stray light, unless the aperture stop itself is carefully designed.[8] Therefore, the black nickel coated aperture stop was made with corrugations to diffusely reflect light away from the intended optical path. During flight in low Earth orbit, the sun will illuminate the instrument from the side. Therefore the baffle was cut at a 45° angle to avoid sunlight entering the instrument. However, the area under the baffle aperture will unavoidably (due to geometrical constraints imposed by the satellite platform) be illuminated by the sun, which can cause light to scatter into the baffle. For this reason, a specular mirror made from diamond turned aluminium was placed at this location to reflect sunlight away from the instrument. The mirror is shown in Figure 7 (but not in Figure 2).

Denoting the spectral radiance seen when looking towards the limb L and the total spectral transmission T, the detected power from a point source inside the FOV can be written as

$$P_{ps}(\theta,\varphi) = \int L(\theta,\varphi,\lambda)\, T(\theta,\varphi,\lambda)\, A_{entr.}\, \Delta\Omega\, d\lambda, \tag{1}$$

where $\Delta\Omega$ is the solid angle in the object plane covered by a single pixel and $A_{entr.}$ is the area of the telescope's entrance pupil. The amount of stray light ending up in the image plane is quantified using the PST, which is defined as the ratio of the irradiance at the baffle entrance and the irradiance in the image plane.[9] Integrating over all directions (excluding the FOV) gives the detected stray light power for a single pixel

$$P_{sl} = \iiint\limits_{4\pi\neg FOV} L(\theta,\varphi,\lambda)\, PST(\theta,\varphi,\lambda)\, A_{pix}\, d\theta d\varphi d\lambda, \tag{2}$$

where A_{pix} is the pixel area. The total signal from stray light sources in each pixel is required to be smaller than the signal due to molecular Rayleigh scattering at an altitude of 85 km (i.e. $\theta_0 = 0.15°$ below the optical axis). A sufficient (although not strictly necessary) requirement for the PST in the most critical region (i.e. below the FOV) can be obtained for an arbitrary wavelength λ_0 assuming $L(\theta,\phi,\lambda_0) = L(\theta,\lambda_0)$ and letting PST be inversely proportional to L, i.e. $PST(\theta,\lambda_0) = \alpha/L(\theta,\lambda_0)$. Using these assumptions with equations 1 and 2 gives (after some manipulation):

$$PST(\theta,\lambda_0) < \frac{L(\theta_0,\lambda_0)T(\theta_0,\lambda_0)}{8L(\theta,\lambda_0)(f/D)^2}. \tag{3}$$

Figure 3 shows how the spectral radiance varies at different altitudes as well as the required maximum in-band PST vs. angular offset from the optical axis. The signal in UV becomes relatively weak at low altitudes, which in turn leads to a less strict PST requirement. The sun has a radiance L_{sun} of approximately $7 \cdot 10^{18}$ photons·cm^{-2}·nm^{-1}·sr^{-1} and covers a solid angle $\Delta\Omega_{sun} = 6.8 \cdot 10^{-5}$ sr. Equation 2 assumes an extended source and is therefore modified to

$$P_{sl,sun} \simeq L(\theta, \varphi, \lambda)\, PST(\theta, \varphi, \lambda)\, A_{pix}\, \Delta\Omega_{sun} \Delta\lambda_{CCD}, \tag{4}$$

where $\Delta\lambda_{CCD} = 500$ nm represents the bandwidth (full-width-half-maximum) of the CCD response. Combining with Equation 1 gives

$$PST_{sun} \lesssim \frac{\frac{\pi}{4} L(\theta_0, \lambda_0) T(\theta_0, \lambda_0) \Delta\lambda_{filter}}{L_{sun} \Delta\Omega_{sun} (f/D)^2 \Delta\lambda_{CCD}}, \tag{5}$$

where $\Delta\lambda_{filter}$ is the bandwidth of the transmission for each channel. The required PST in the direction of direct illumination of the sun becomes $8.7 \cdot 10^{-12}$ and $1.2 \cdot 10^{-10}$ for the UV1-UV2 and IR1-IR4 channels, respectively.

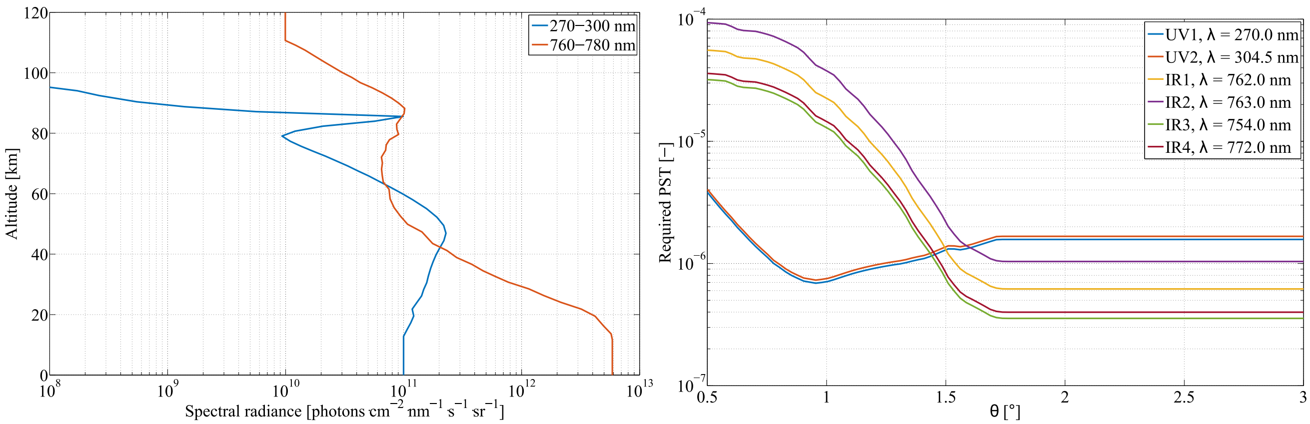

Figure 3. Altitude vs. measured spectral radiance in the wavelength regions 270-300 nm and 760-780 nm (left) and required maximum PST vs. θ (for $\varphi = 270°$) (right). See Figure 7 for coordinate convention.

3. BAFFLE BREADBOARD

As part of the effort of establishing an efficient system for stray light suppression, a simplified baffle breadboard model was produced and tested. The purpose of this effort was to compare actual measurements to stray light simulations as well as evaluating the newly built facility for stray light measurements in the MATS project. A rectangular 700 mm × 140 mm × 80 mm aluminium tube was used to build the baffle, which had four equidistant baffle vanes with knife-edge apertures that match the instrument's FOV (see Figure 4). Just like the baffle for flight, the inside of the breadboard baffle was coated with Vantablack S-VIS.

Stray light simulation models were created in Opticstudio and Lighttools, where scattering from the surfaces coated with Vantablack S-VIS were modeled using empirical BRDF curves, supplied by the manufacturer. The measured curves were acquired using white light at four different angles of incidence (10°, 30°, 50° and 70°). This data was implemented and used in simulation models in both optical softwares. A collimated source at 500 nm was used in the models to illuminate the entire baffle front aperture at different angles of incidence while the amount of scattered light reaching the back aperture was recorded.

A new facility for stray light and imaging performance measurements has been built at Omnisys Instruments. The room itself is a 8.5 m × 4.5 m darkroom where the stray light source and the test object were placed at opposite sides of the room some 6 m apart. The room was separated into three equally sized sections using two rubberized blackout curtains (Thorlabs BK5) that span across the entire short side of the room. Holes of approximately the same size as the baffle front aperture were made in the middle of both curtains to enable only one direct path between the source and the test object. This in combination with the relatively low reflectance

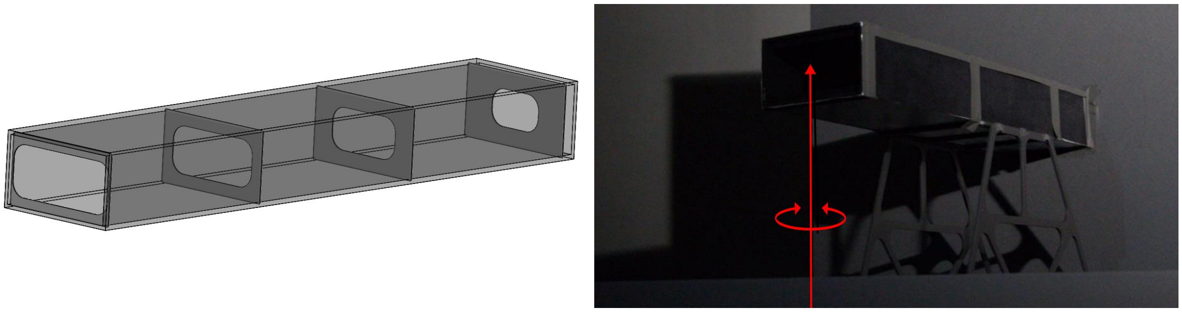

Figure 4. CAD model of the baffle breadboard showing the four knife-edge vanes installed on its inside (left) and a photo showing the baffle breadboard mounted in the stray light test setup (right). The rotation axis of the baffle is indicated with a red arrow.

(4-5%[10]) of the blackout curtains made sure to block unwanted light paths and thereby provided a low light level around the test object.

It is very important to minimize the amount of dust in the air, which scatters light and thereby adds to the overall background noise/uncertainty in the measurement. Cleanliness is of course also important in order not to contaminate the instrument during the various test campaigns. A series of measures were therefore taken to establish a facility that was as clean as possible with relatively simple means. For example: an airlock/gowning area outside the lab was built where all-covering cleanroom clothes were put on and worn at all times while in the lab. Daily cleaning of the floors using cleanroom-certified dry wipes was done. Dust filters were installed in the air intake and a portable HEPA fan for filtration was placed inside the lab. Recently, the lab has also been equipped with a clean room tent that has a fan with HEPA filter installed on the top to provide a laminar flow of clean air around the test object. To quantify how different behaviors of the workers inside the lab affected the amount of dust in the air, a particle counter was used while recording different actions. In this test, a person was first walking around inside the lab with both the HEPA fan and the house ventilation turned on. The person then left and, later, the house ventilation was turned off. Finally, the HEPA fan was also turned off. Figure 5 shows the results, which clearly indicate that the best conditions are obtained with the external ventilation turned off and the portable HEPA filter turned on. Hence, all stray light measurements were therefore programmed to start at nighttime, long after the last person left the lab, and at least six hours after the house ventilation was turned off. The particle counter used was only able to measure dust down to 0.5 um and it is therefore not possible to truly claim a cleanliness level below ISO 7. However, as can be seen in Figure 5, the requirements for particles larger than 0.5 um are well below those needed for ISO 5. Results from other groups show that facilities with ISO 5 classification[11] are able to measure a PST down to 10^{-9}.

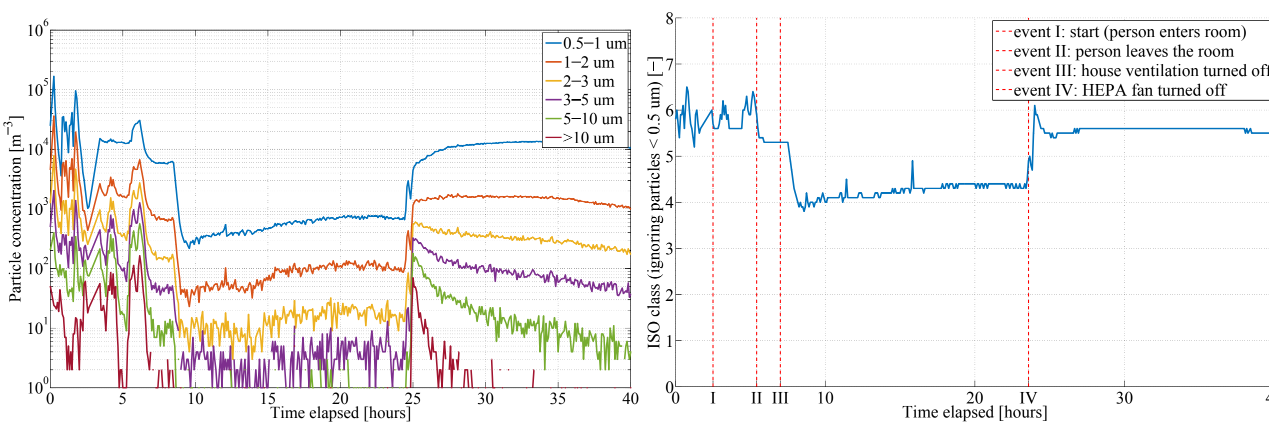

Figure 5. Measurement of particle concentration inside the stray light measurement lab (left) and corresponding ISO class (right). Note that the calculated ISO class is an estimate since particles smaller than 0.5 um were not measured.

A 1 kW Xe source with an ozone-free lamp (Sciencetech, XLH–S–1000X) was used together with a parabolic mirror in an off-axis configuration to achieve collimation of the beam that illuminates the baffle front aperture. The baffle was mounted on a rotary stage so that the incident azimuth angle could be varied during the measurements. A room temperature Si photomultiplier (Hamamatsu, S13360-6050CS) with a 6 mm × 6 mm photosensitive area was used to record the power transmitted through the baffle. This detector was mounted on linear stages and scanned in a meander pattern across the entire back aperture. To further reduce the amount of unwanted reflections from the room, black plates were mounted next to (but not behind) the detector. Reflections from the detector housing and its immediate surroundings were minimized by using light absorbing sheets (Acktar, Metal Velvet), which have a hemispherical reflectance <1% across the operating wavelengths of the detector.

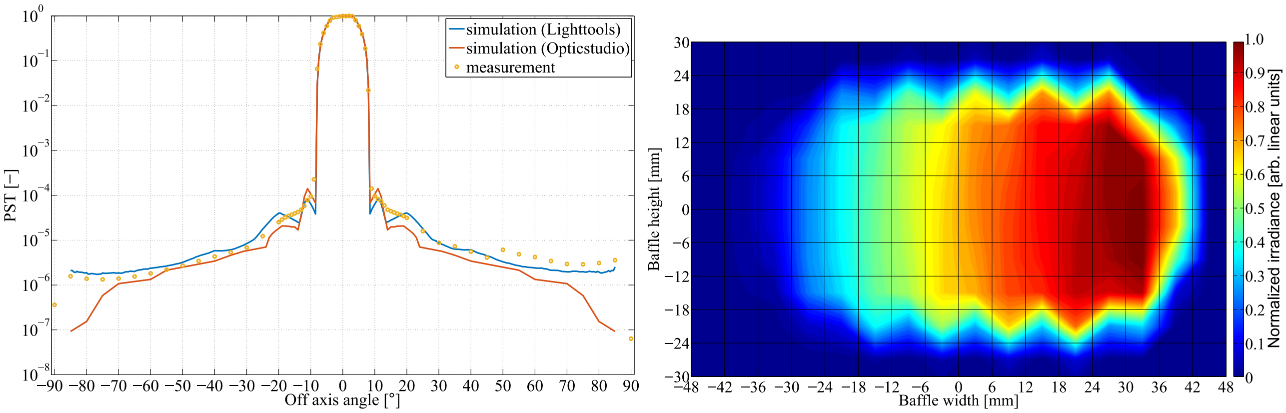

Figure 6. Measured and simulated PST of the breadboard baffle (left) and sample of scattered light measured at the back aperture of the baffle for a 40° angle of incidence (right).

A stack of neutral density (ND) filters were attached to the detector in order to avoid saturation at angles close to the baffle's symmetry axis. Several measurement sets with varying amounts of attenuation were used and matched for overlapping angles of incidence. The results from these measurements and the corresponding simulations are shown in Figure 6. As can be seen, there is a close agreement between simulations and measurements. It is also clear that the facility is capable of measuring a PST down to at least 10^{-6}. The slightly higher PST that was measured at off-axis angles > 0 are attributed to a damage that happened at the front of the baffle. Some of the Vantablack coating was peeled off due to a mistake in handling, which led to more light being reflected into the baffle. This damage was covered with low-reflectance tape, but the effect could not be removed completely.

4. STRAY LIGHT SIMULATIONS OF LIMB INSTRUMENT PROTOTYPE

It is a very complex and time-consuming task to measure the stray light suppression capability of the limb instrument for each possible angle of incidence. Therefore, it was decided to take an approach where stray light is measured for the most critical angles of incidence (see Section 2), but where detailed simulations will ultimately be the path to knowing the stray light suppression capability of the instrument. The simulations performed in this section are done for a prototype model, which is highly representative of the final flight model.

In order to properly analyze the stray light suppression of the limb instrument payload, a simplified version of the mechanical CAD model (shown in Figure 2) was made. This model was entirely representative in terms of dimensions and crucial components, but without unnecessary details (e.g., screw threads) that otherwise tend to make stray light simulations unbearably time-consuming. The CAD model was imported into a model created in Opticstudio, which also included all optical components with measured spectral properties. However, only data for the total transmission of each component were available at the time when the model was being set up. Therefore, an anti-reflection (AR) coating of 1% across all wavelengths were assumed for the backside of the glass components. Simulations with ideal AR coatings were also performed.

Figure 7 shows the Opticstudio model as well as the actual limb instrument hardware prototype it was based on. The scattering model used for the baffle coated with Vantablack S-VIS was the same as for the breadboard simulations, whereas the simpler Lambertian scattering model was used for the other surfaces coated with black nickel. Modeling scatter from the diamond turned aluminium mirror in front of the baffle is difficult since toolmarks from the machining make the surface non-isotropic. Hence, scattering models, such as Lambertian or ABg, become invalid.[12] As a conservative approach to this problem, the highly specular mirror was instead modeled as a fully Lambertian surface. Although incorrect, this approach was deemed to provide an upper limit of the amount of stray light, even though potential structures stemming from diffracted light will not be seen in the analysis.

For each of the six channels of the limb instruments, stray light simulations were performed at five points corresponding to the peak transmission (cf. Table 1) as well as the 50% and 90% transmission levels on both sides of the center wavelength. In addition, three out-of-band wavelengths (200, 500 and 1100 nm) corresponding to the mid band and outer flanks of the CCD sensitivity curves were also included in the simulation. All simulations were entirely based on ray tracing methods, and effects of diffraction are therefore not considered. This implies that $PST = 0$ in all directions, corresponding to the negative half sphere seen from the instrument's optical axis. Hence, these directions were never considered in the analysis.

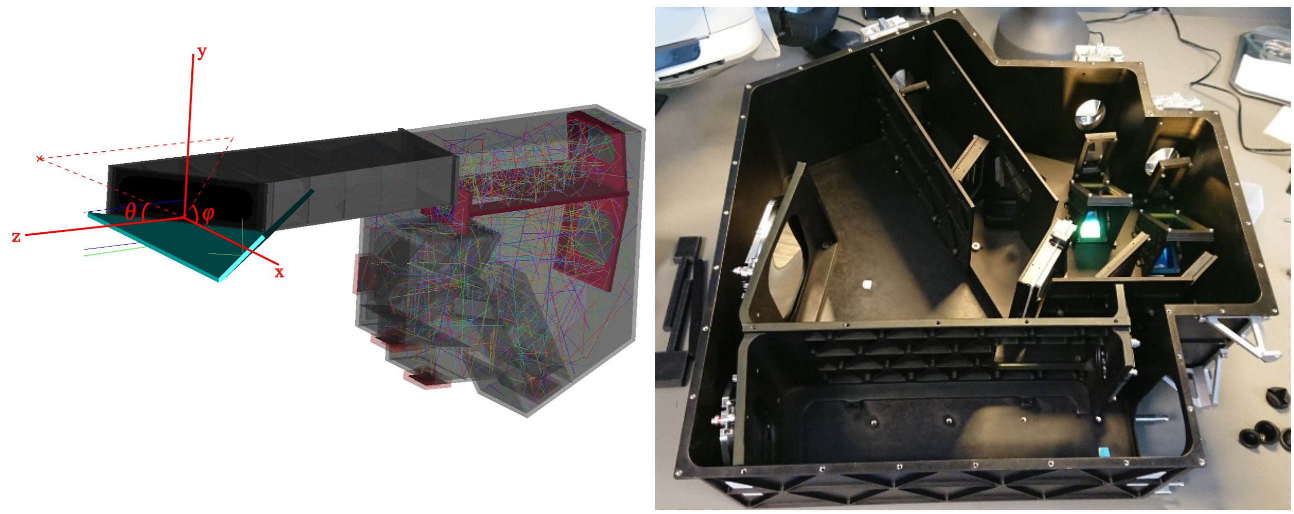

Figure 7. To the left: Opticstudio stray light model with light scattered on its inside. The coordinate convention used in the stray light analysis is indicated in red. The turquoise structure beneath the baffle aperture is the mirror to reflect sunlight away from the instrument. To the right: Photo of limb instrument prototype during assembly.

A batch processing script to control Opticstudio was written in Matlab to sweep over wavelength and angle of incidence. In order to resolve minute details in the simulated PST, rays with energies down to a fraction 10^{-10} of the launch energy were traced before being terminated by the program. In each step of the simulation, a total of 10^6 rays were traced. These numbers were chosen on the basis of a convergence analysis in which the simulated PST was investigated as the ray threshold energy and number of rays were varied.

The left part of Figure 8 shows the simulated PST vs. θ in the most critical region for stray light (i.e. just below the optical axis towards the ground). The average PST is well below the required level for $\theta > 2.5°$ (c.f. Figure 3), but the maximum PST is too high closer to the optical axis. Analyzing how the stray light suppression varies in the image plane for a given angle of incidence revealed clear structures in the simulated PST – see Case I, Figure 10. As can be seen, several clearly distinguished maxima are present. In order to determine which maxima can be attributed to the 1% AR coating at the back of the glass components, the simulations were repeated with ideal AR coatings (Case II). The results are shown at the third and fourth row of frames in Figure 10. As expected, the overall signal goes down with ideal AR coating, but several noticeable patterns also disappear in all channels. However, it was clear that one maximum in the center still remained in each frame.

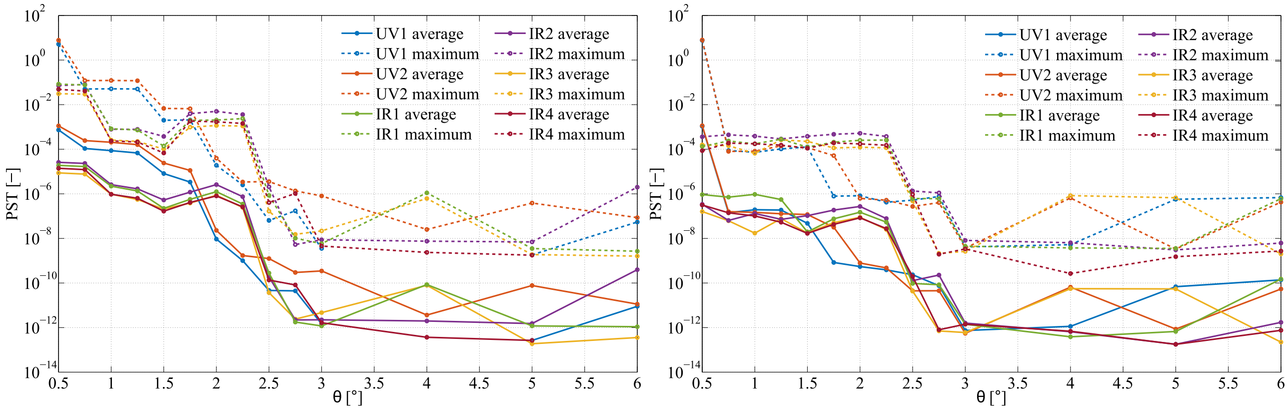

Figure 8. PST vs. θ (for $\varphi = 270°$). Case I: a 1% reflectance on the backside of all glass components (left). Case III: ideal AR coating and increased beamsplitter-filter separation (right).

Analyzing the ray paths in more detail revealed two design flaws of the instrument prototype, which explain the remaining patterns in the image planes. As illustrated in Figure 2, both the beamsplitter for the two UV channels and the beamsplitter following after M3 are situated close to a broadband filter. With this arrangement, some of the light that passes through the beamsplitter is reflected off one of the surfaces of the broadband filter and then reflected off one of the surfaces of the beamsplitter before being transmitted through the broadband filter. This results in one or several offset ghost images as shown in Figure 10. A simple remedy for this problem is to increase the separation between the beamsplitters and the broadband filters. The right part of Figure 8 and fifth and sixth rows in 10 (Case III) show the resulting PST from this change, which will also be implemented in the flight instrument.

When analyzing the stray light simulations at 500 nm, it became clear that the short distance between the beamsplitter succeeding M3 and the broadband filter behind it implied an increased stray light level in the UV channels. It turned out that visible light transmitted through the beamsplitter is reflected of the surface of the broadband filter and to a large extent directed towards the UV channels. The separation of these two components helped to direct the light towards black-coated surfaces where it could be absorbed.

Comparing the simulated PST for different channels in figures 8 and 10, it is clear that the UV are the most sensitive to in-band stray light. Higher reflectivity of black nickel at shorter wavelengths contributed to this result. Comparing the UV channels, it can be seen that the UV2 channel has a slightly higher stray light throughput than the other channels. This fact was attributed to the location of the UV2 channel, which is less embedded – and therefore more susceptible to critical paths – than other channels. For this reason, the UV2 channel was analyzed in terms of stray light from the sun. A source with a total number of 10^6 rays with relative energies down to 10^{-16} was used to illuminate the surface below the baffle aperture. This surface was modeled as a Lambertian scatterer with 100% reflectivity. The PST in the image plane of the UV2 channel is $1.1 \cdot 10^{-11}$ - cf. Figure 9. It is therefore deemed very likely that the flight instrument will be compliant with the stray light suppression requirement since a diamond turned mirror will take the place of the diffuse scatterer used in the simulation.

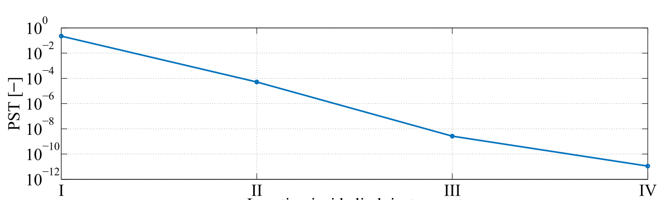

Figure 9. PST at four different locations inside the limb instrument: I – baffle front aperture, II – baffle back aperture, III – UV2 narrowband filter, IV – UV2 image plane. Simulations performed at $\lambda = 304.5$ nm at $\theta = 60°$, $\varphi = 140°$. The surface below the baffle front aperture was modeled using Lambertian scattering.

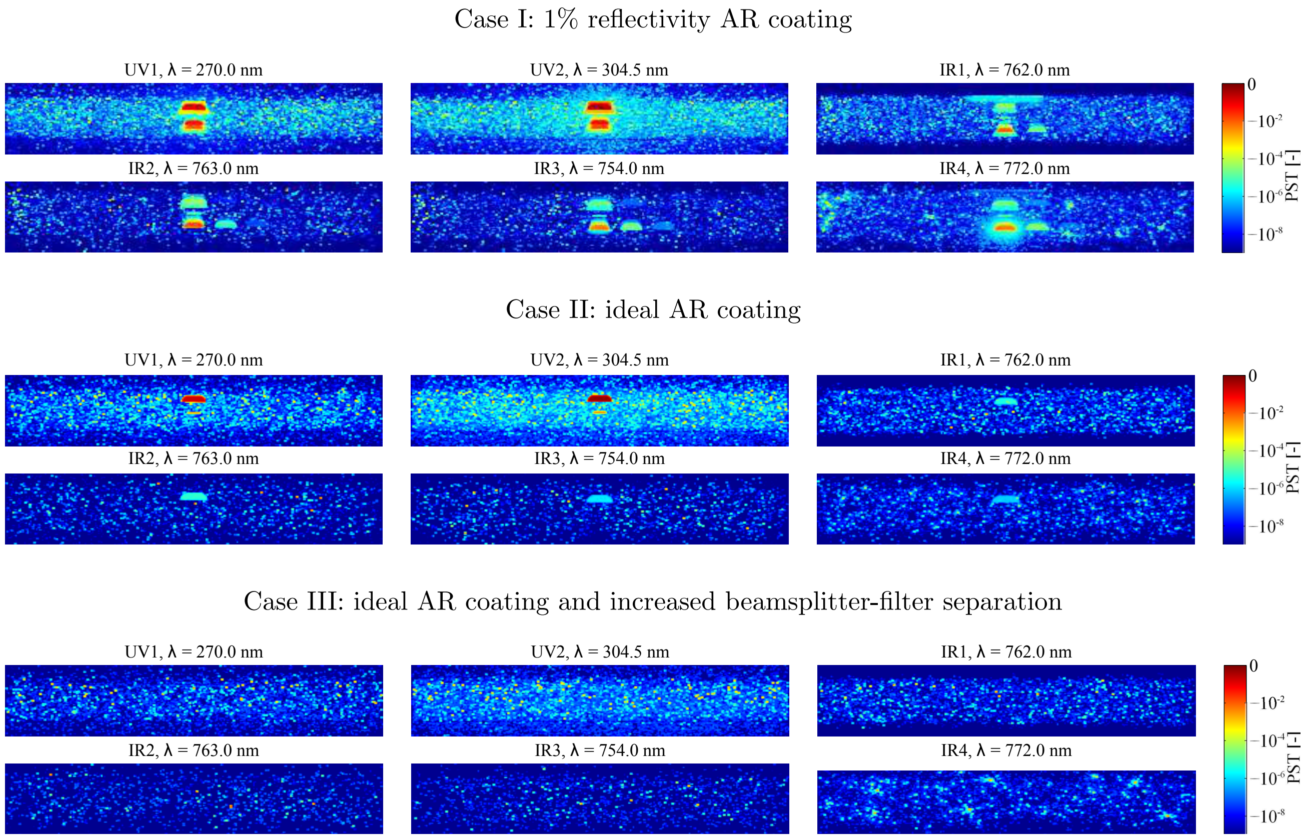

Figure 10. Simulated PST frames for all channels at the respective center wavelength at $\theta = 1.5^\circ$ and $\varphi = 270^\circ$. The size of each frame is 27.6 mm $\times$ 6.9 mm.

5. INSTRUMENT MODEL AND IN ORBIT PERFORMANCE

During operation in space, the uncertainty in the data recorded by the MATS instrument will depend on a multitude of factors besides stray light. It is therefore important for the end users to understand and be able to study how the instrument behaves under given conditions (e.g. beginning/end of exposure, temperature, stray light levels etc.). Hence, a software instrument model was written to analyze every important function and feature of the instrument. This includes stray light suppression, imaging performance, temperature dependent spectral selection, noise in the image sensors, etc. At the time of writing, the first version of the instrument model had just been finished and below follows a description of the program as well as some preliminary results. Even though the code is written with the MATS satellite in mind, it is written in a general way and can be adjusted for other optical instruments. After more testing, the instrument model is intended to be made available to the public under an open-source license.

The code was written in Python and uses an object-oriented programming style. It takes a series of input frames and outputs a set of images corresponding to those that will be sent to Earth during operation of the satellite. Each input frame is represented by a two-dimensional radiance matrix that has a corresponding wavelength, time stamp and coordinate vectors. Besides the frames representing radiation from within the FOV, a set of stray light frames can also be inputted to the program. Exactly how each frame is then manipulated by the software can be fully controlled by the user, but a typical execution is intended to mimic how the light travels through the instrument towards the sensors and is finally read out by the on board computer of the satellite. This means that depending on which of the six channels is being analyzed, a specific light path towards the image sensor is selected. A unique transmission vs. wavelength vector is defined, which scales the input signal level. A set of point spread functions (PSF) is used for each specific channel. These were generated from simulations in Opticstudio, where the shape of the three telescope mirrors were modeled based on surface metrology of the fabricated flight mirrors. Besides providing a description of the resolution of the image, the PSF data also provides the correct scaling and mapping of a point source in the object plane to the image plane. Thus, the code incorporates relative illumination and distortion automatically. Stray light is implemented in a way similar to imaging, but instead of using a PSF to map a single point source inside the FOV to a limited region in the image plane, the PST distributions are used to map all sources outside the FOV to the whole image plane (c.f. equations 1 and 2).

The CCD image sensors are treated as separate objects, which accept a number of input frames that have units of irradiance. All frames are cropped to match the unmasked region of the sensor. The physical pixel area and exposure time are taken into account to change the units to counts/number of electrons. Shot noise, readout noise and dark currents (temperature-dependent) are added to the output frame. Finally, the readout process is simulated, which includes effects of saturation, on-chip binning and smearing. The latter effect arises since the limb instrument lacks a mechanical shutter, which causes the sensors to be illuminated during the readout process.

A sample image generated by the instrument model is shown in Figure 11. Barrel distortion can be seen by noticing the curvature of the outer region of the image. Effects of sensor noise and smearing during readout are seen more clearly in the right part of Figure 11, which is displayed in logarithmic scale. No on-chip binning was applied, even though this will be the case for the instrument during operation.

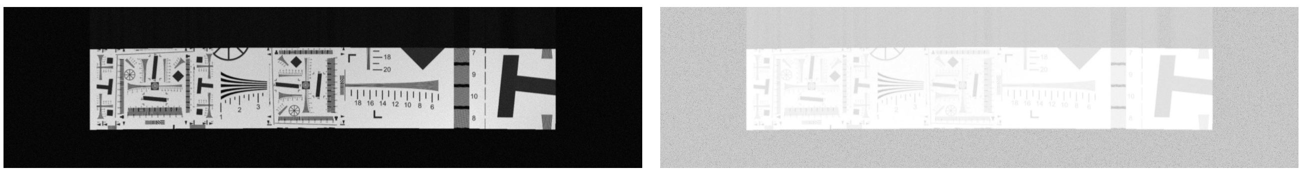

Figure 11. Instrument model sample image in linear (left) and logarithmic scale (right). The size of each frame is 27.6 mm $\times$ 6.9 mm.

As a second example, a software-generated[13] atmospheric scene with gravity waves was used as input to the instrument model – see Figure 12. The IR1 channel was used in the simulation and input parameters to the instrument model were chosen to be as realistic as possible. Hence, the exposure time was set to 3 s and on-chip binning factors of 2 and 5 were used in the vertical and horizontal direction, respectively. A weighted average of the two input frames was calculated by the instrument model to approximate the scene during exposure. The temperature of the image sensors set to -10° C. This resulted in an output image from the instrument model, which is shown in Figure 13. As can be seen, the wave structures of the input image are clearly resolved, although some degradation of the image quality has clearly occurred. This is mostly due to the on-chip binning rather than the imaging performance itself. As the operating temperature of the image sensor is low and the input relatively bright, dark currents are barely seen. The slightly increase in brightness in the upper part of Figure 13 is due to the aforementioned smearing effects. These are to some extent deterministic and can therefore be partly removed in the data post-processing.

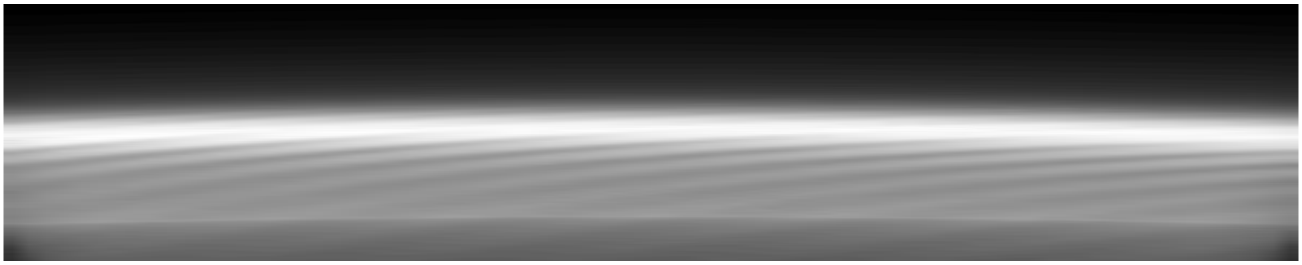

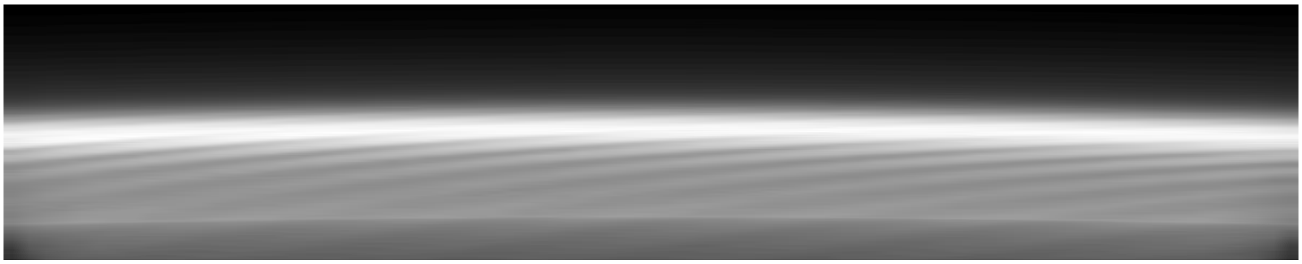

Figure 12. Images of simulated atmospheric gravity waves as seen from the satellite point of view at a 585 km altitude (cf. Figure 1). The two frames cover 4.71° × 0.94° and show the same atmospheric scene at two instances, 60 s apart.

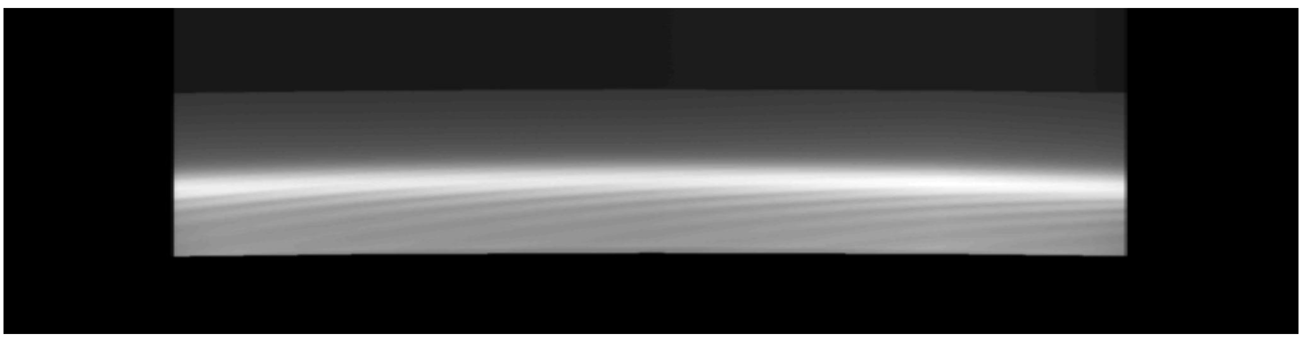

Figure 13. Output image from the instrument model using the IR1 channel. The size of the 2048 × 512 pixel frame is 27.6 mm × 6.9 mm.

6. CONCLUSION

Simulations and measurements have been combined to investigate the stray light suppression capability of the limb instrument of the MATS satellite. In particular, a baffle prototype coated with Vantablack S-VIS was produced and tested. The measurements revealed a PST down to 10^{-6}, which is in excellent agreement with simulations performed in two optical softwares (Opticstudio and Lighttools). These results also show that the dynamic range of the newly built facility for stray light measurements should be sufficient to measure the PST of the instrument for flight.

Based on the results from the baffle breadboard, detailed stray light analysis of a prototype model of the limb instrument was performed using Opticstudio. The region below the instrument's nominal FOV is the most critical and was therefore analyzed in detail. It was clear from the stray light analysis that some minor updates to the instrument are needed to remove excess stray light and ghost images. Simulations showed that the stray light suppression requirement are met when the changes are implemented.

An instrument model that simulates the performance of MATS in space was written and tested. Preliminary results showed that wave structures in the atmosphere were clearly resolved, while sensor noise levels were relatively low with the given brightness of the input scene.

ACKNOWLEDGMENTS

This research was partially funded by the Erna and Victor Hasselblad Foundation. The MATS satellite is funded by the Swedish National Space Board (SNSB).

REFERENCES

[1] Larsson, N., Lilja, R., Gumbel, J., Christensen, O. M., and Örth, M., "The MATS micro satellite mission – tomographic perspective on the mesosphere," in [*The 4s Symposium 2016*], 11070–11078, ESA Conference Bureau (May 2016).

[2] Karlsson, B. and Shepherd, T. G., "The improbable clouds at the edge of the atmosphere," *Physics today* **71**(6), 30–36 (2018).

[3] Mendenhall, J. A. and Lencioni, D. E., "EO-1 Advanced Land Imager stray light analysis and impact on flight data," in [*IEEE International Geoscience and Remote Sensing Symposium*], **6**, 3114–3117 vol.6 (June 2002).

[4] Mohammad Asadnezhad, Abdollah Eslamimajd, H. H., "Stray light analysis, baffle, and optical design of a high-resolution satellite camera," *Journal of Applied Remote Sensing* **12**, 12 – 12 – 16 (2018).

[5] Park, J.-O., Jang, W.-K., Kim, S.-H., Jang, H.-S., and Lee, S.-H., "Stray light analysis of high resolution camera for a low-Earth-orbit satellite," *J. Opt. Soc. Korea* **15**, 52–55 (Mar 2011).

[6] Giono, G., Olentšenko, G., Ivchenko, N., Christensen, O. M., Gumbel, J., Frisk, U., Hammar, A., Davies, I., and Megner, L., "Characterisation of the analogue read-out chain for the CCDs onboard the mesospheric airglow/aerosol tomography and spectroscopy (MATS)," *Proc.SPIE* **10698**, 10698 – 10698 – 8 (2018).

[7] "Vantablack data brochure." Surrey Nanosystems https://www.surreynanosystems.com/assets/media/vantablack-s-vis-a4-data-brochure-2017-026.pdf (Accessed: September 11, 2018).

[8] Mazzoli, A., Holbrouck, P., Houbrechts, Y., Maresi, L., Stockman, Y., Taccola, M., and Versluys, J., "Baffles design of the PROBA-V wide FOV TMA," *Proc.SPIE* **10565** (2017).

[9] Breault, B. P., [*Handbook of Optics*], McGraw-Hill, New York (1995).

[10] Marshall, J. L., Williams, P., Rheault, J.-P., Prochaska, T., Allen, R. D., and DePoy, D. L., "Characterization of the reflectivity of various black materials," *Proc. SPIE, Ground-based and Airborne Instrumentation for Astronomy V, 91474F* (2004).

[11] Fleming, J., Grochocki, F., Finch, T., Willis, S., and Kaptchen, P., "New stray light test facility and initial results," *Proc.SPIE* **7069** (2008).

[12] Pfisterer, R., "Approximated scatter models for: Stray light analysis," *OPN Optics & Photonics News* **22**, 16 – 17 (October 2011).

[13] Li, A., *A 3D-model for O2 airglow perturbations induced by gravity waves in the upper mesosphere*, Master's thesis (2017).